J. Fluid Mech. (1994), *vol.* 259, *pp.* 191–218

Wall shear stress and velocity in a turbulent axisymmetric boundary layer

By ANTHONY WIETRZAK AND RICHARD M. LUEPTOW
Department of Mechanical Engineering, Northwestern University, Evanston, IL 60208, USA

(Received 14 September 1992 and in revised form 4 March 1993)

Instantaneous streamwise fluctuations of the wall shear stress have been measured using a hot-element probe in a thick axisymmetric turbulent boundary layer on a cylinder aligned parallel to the flow. The measurements were made at a momentum-thickness Reynolds number $R_\theta = 3050$ and a ratio of boundary-layer thickness to cylinder radius of $\delta/a = 5.7$. The ratio of the r.m.s. of the fluctuation to the mean value of the wall shear stress, $\tau_{rms}/\bar{\tau}$, is about 0.32, a value slightly lower than that for recent measurements for flow over a flat plate. The probability density function of the wall shear stress is similar to that for planar wall-bounded flows within experimental error. The power spectral density of the wall shear stress shows that a cylindrical boundary layer contains less energy at lower frequencies and more energy at higher frequencies than other wall-bounded flows. Analysis of simultaneous measurements of the streamwise wall shear stress and the streamwise velocity using VITA and peak detection suggests that transverse curvature has little effect on the near-wall burst–sweep cycle compared to planar wall-bounded flows. The angle of inclination of the structures is similar to that measured for large-scale structures in planar wall-bounded flows. However, measurements of the cross-correlation between the shear stress and the velocity suggest the existence of smaller structures yawed to the axis of the cylinder. The coherence between shear stress and velocity shows a low frequency associated with the inclined structures and a higher frequency associated with the yawed structures. The yawed structures could have an arrowhead or half-arrowhead shape and may be associated with fluid from the outer flow washing over the cylinder.

1. Introduction

The effect of transverse curvature on the turbulent boundary layer that develops as a fluid flows parallel to a cylindrical surface has applications to boundary layers on many different bodies including missiles, towed submerged cables, vehicles, and glass or polymer fibres during fabrication. Even though the instantaneous structure of turbulent planar wall-bounded flows has been investigated in great detail in an effort to understand the dynamics of the flow (Robinson 1990), the effects of transverse curvature on the flow have been largely neglected. The analysis of a boundary layer with transverse curvature, such as the boundary layer on a cylinder in axial flow, is complicated by the additional lengthscale related to the transverse curvature of the wall and the fact that the boundary-layer thickness δ can grow to be much larger than the radius of the cylinder a.

The character of a cylindrical turbulent boundary layer has a strong dependence on the parameter δ/a, relating the boundary-layer lengthscale to the curvature of the wall. For $\delta/a < O(1)$, the measurements of turbulence intensity, Reynolds stress, and wall-

pressure fluctuations appear similar to those of other wall-bounded flows indicating that transverse curvature plays little role in the structure of the turbulence (Willmarth & Yang 1970; Willmarth *et al.* 1976; Luxton, Bull & Rajagopalan 1984; Lueptow 1990). However, the effect of transverse curvature becomes apparent in the fuller mean velocity profile and higher coefficient of friction for $\delta/a > O(1)$ (Richmond 1957). The Reynolds stress drops off more quickly with distance from the wall than in a planar boundary layer, perhaps as a result of spreading of the flow field to larger circumferences from the wall to the edge of the boundary layer (Lueptow, Leehey & Stellinger 1985). The wall-pressure spectrum contains a lower energy density at low frequencies than planar wall-bounded flows (Willmarth & Yang 1970). A striking difference between the boundary layer on a cylinder and that on a flat plate is that the wall of the cylinder does not constrain the motion of turbulent eddies in the wall normal direction as much as a flat plate. Flow visualization of a cylindrical boundary layer indicates that large turbulent structures can pass from one side of a cylinder to the other when the cylinder diameter is small in comparison to the boundary-layer thickness (Lueptow & Haritonidis 1987). Consequently, the turbulent character of the cylindrical boundary layer is boundary-layer-like in the immediate vicinity of the wall and wake-like further away from the wall when δ is much larger than the cylinder radius.

An issue that still remains the subject of controversy for wall-bounded flows is the connection between the bursting phenomenon near the wall and the large-scale motion observed in the outer part of a turbulent boundary layer (Robinson 1990). Distinct and well-defined bursts of low-momentum fluid ejected away from the wall followed by sweeps of high-speed fluid from the outer regions towards the wall are responsible for most turbulence production in planar wall-bounded flows (Kline *et al.* 1967; Corino & Brodkey 1969; Kim, Kline & Reynolds 1971). Application of turbulence detection schemes for the analysis of bursts to the turbulent boundary layer on a cylinder in axial flow indicates that the conditionally averaged events are similar to those for a flat plate. However, the outer wake-like portion of the boundary layer may promote the bursting process (Lueptow & Haritonidis 1987).

The instantaneous wall shear stress is a signature of the phenomena occurring above it. Hence, the effects of the transverse curvature on the structure of a cylindrical boundary layer should be reflected in the instantaneous values of the wall shear stress. The purpose of this investigation is to determine the character of the streamwise fluctuating wall shear stress as well as to relate the fluctuating wall shear stress to the streamwise velocity in a cylindrical turbulent boundary layer. Unfortunately, the characteristics of the fluctuating wall shear stress are not well established even for the turbulent boundary layer on a flat plate. Although several measurements of the wall shear stress intensity, $\tau_{rms}/\bar{\tau}$, have been made (as noted in table 2), there is no consensus on its value. This may be a result of the use of several different techniques for measuring the wall shear stress, each having its own problems with spatial resolution and frequency response. Even fewer reliable measurements have been made of the wall shear stress simultaneously with the velocity in planar boundary layers, and none have been made in cylindrical boundary layers.

In this paper we present results of measurements of the fluctuating wall shear stress in the boundary layer on a cylinder in axial flow as well as simultaneous wall shear stress and streamwise velocity measurements. The purpose of this work is to understand the effect of transverse curvature on the structure of the turbulence in a boundary layer on a cylinder in axial flow as well as to address the fundamental relationship between the wall shear stress and the velocity field.

2. Experimental arrangement

2.1. *Vertical wind tunnel*

This investigation was conducted in the vertical wind tunnel facility at Northwestern University. A schematic of the wind tunnel including an exploded view of the cylindrical model and the velocity/shear probe arrangement is shown in figure 1. This open-circuit wind tunnel has a test section 3.05 m long with a 0.364×0.364 m square cross-section. At a normal air speed of 10 m s^{-1} the level of free-stream turbulence in the wind tunnel was 0.15% in the frequency range from 0.1 to 20000 Hz. The pressure gradient along the length of the test section was negligible. More details of the wind tunnel can be found in Wietrzak (1992) and Snarski (1992).

2.2. *Cylindrical model*

A 3.0 m long cylinder suspended along the centreline of the test section was used for all of the experiments. The cylinder was fabricated from an acrylic tube of 0.952 ± 0.0063 cm outer diameter and a wall thickness of 0.159 cm. The low thermal conductivity of the acrylic reduced the effects of the heat transfer to the wall from the hot-wire velocity probe, allowing velocity measurements to be made closer to the wall. The test cylinder was placed in tension to ensure its straightness and stability during the tests conducted. To assure axial symmetry of the boundary layer, the wall shear stress was measured using a Preston tube (Patel 1965; Head & Ram 1970) of 0.56 mm OD and 0.15 mm wall at the same axial position but different circumferential locations. The variation in wall shear stress was less than 4%, indicating a high degree of axial symmetry of the boundary layer.

A 1.250 cm OD O-ring around the leading edge of the cylinder at the upstream end of the test section was used to trip the boundary layer. The wall shear stress measurements were made 2.10 m downstream of the trip. The characteristics of the boundary layer at this location along with other measurement parameters are given in table 1.

2.3. *Instrumentation*

Mean and fluctuating velocities were measured using a home-built hot-wire U probe that was mounted at the tip of an airfoil sting that could be traversed along the length of the wind-tunnel test section. The sensing wire was a 2.5 μm diameter Pt–Rh (90/10) alloy. The length of the sensing wire was 0.051 cm. This corresponded to the ratio of sensing length to wire diameter $l/d = 203$, and $l^+ = 17.0$ at a free-stream velocity of 11 m s^{-1}. The + superscript denotes non-dimensionalization with the friction velocity u_τ and kinematic viscosity ν. Thus, the criterion that $l/d \geqslant 200$ in order for the effects of heat loss to the prongs to be negligible was satisfied as was the criterion recommended by Blackwelder & Haritonidis (1983) that $l^+ = 10$–20 for adequate spanwise spatial resolution. The shear probe used to measure the instantaneous wall shear stress is described in detail in §3.

The hot-wire probe and the shear probe were operated using a DANTEC model CTA 56C01/56C17 constant-temperature anemometer. Both probes were operated at a resistance overheat ratio of 30%. This overheat ratio has been used successfully with wire-on-the-wall-type shear probes by other investigators (Alfredsson *et al.* 1988; Shah & Antonia 1987). The standard square-wave test gave a frequency response of 22 kHz and 17 kHz for the velocity probe and shear probe, respectively.

The hot-wire probe was always calibrated in the free stream of the wind tunnel just prior to recording the data. The wind tunnel was run at 5 to 10 different free-stream

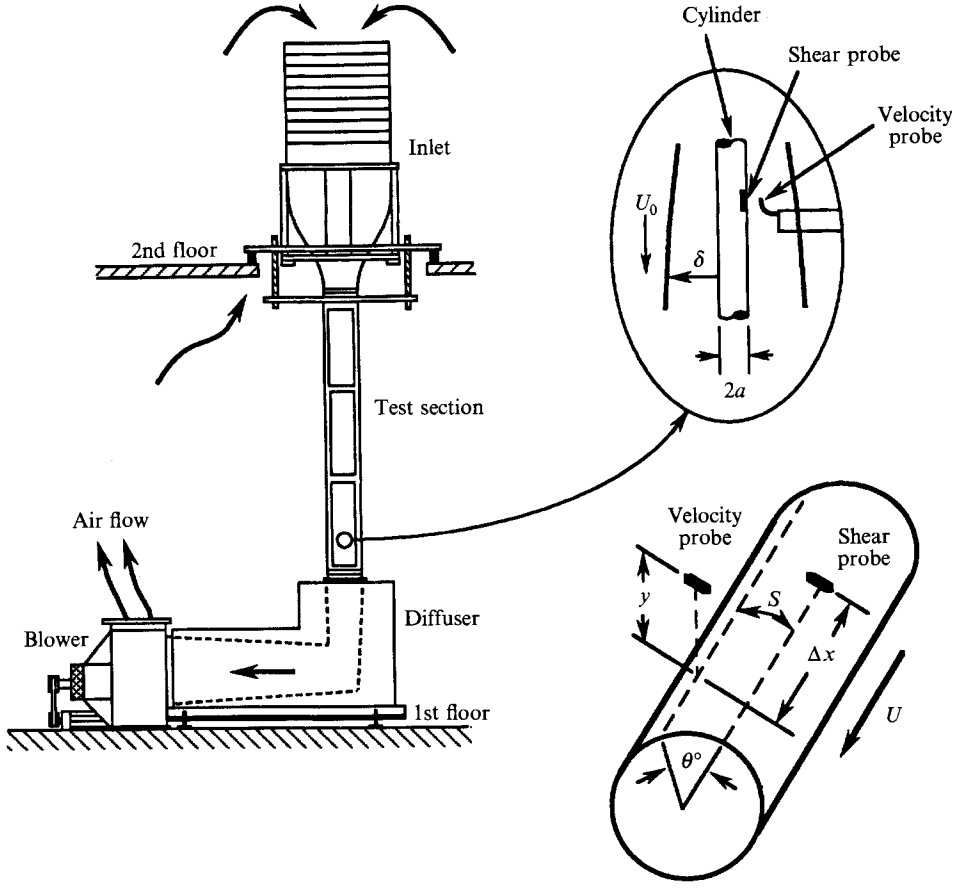

FIGURE 1. Schematic of the wind tunnel and velocity/shear probe arrangement.

U_0	$= 11.0$ m s^{-1}
$\delta_{0.99}$	$= 2.70 \pm 0.18$ cm
δ^*	$= 0.491 \pm 0.07$ cm
θ	$= 0.423 \pm 0.058$ cm
Re_θ	$= 3050$
$\bar{\tau}$	$= 0.307$ Pa
u_τ/U_0	$= 0.046$
$\Delta t^+ = \Delta t u_\tau^2/\nu$	$= 0.84$
$l^+ = lu_\tau/\nu$	$= 17$ (velocity probe)
$W^+ = Wu_\tau/\nu$	$= 9$ (shear stress probe)

TABLE 1. Characteristics of flow and measurements. Note that δ^* and θ denote the displacement and momentum thickness, respectively, using the cylindrical boundary layer definition (Kelly 1954).

velocities. The free-stream velocities were measured using a Pitot tube and a BARATRON-223-B differential pressure transducer with a resolution of 0.001 mm Hg. A third-order polynomial was used to fit the anemometer's voltage to the velocity. The calibration was repeated after data were taken, and the data were discarded if the calibration changed by more than 2%.

In all cases, prior to sampling, the d.c. voltage outputs from the anemometer were

first offset and then the signals were amplified, using home-built electronics, with gains of approximately 80 and 180 for the velocity probe and the shear probe, respectively. The data to be used in the analysis were sampled at 20 kHz after being low-pass filtered at the Nyquist frequency of 10 kHz. The non-dimensional time between samples, Δt^+, is shown in table 1.

The data were digitized using a 12-bit GWI-625 MacADIOS II A/D board in a Macintosh IIcx computer. The temporal sampling length per data set was $1700\delta/U_0$ (80000 points). Since the time for the passage of a large eddy in the outer flow is of the order δ/U_0 this represents the time for passage of several hundred large eddies. Some data sets with a temporal sampling length of $21000\delta/U_0$ (10^6 points) were also taken.

3. Heated-element shear probe

3.1. *Background*

Most successful measurements of the fluctuating wall shear stress in pipes or planar wall-bounded flows have utilized heat transfer or mass transfer shear probes. Excellent reviews of the subject are given by Dewey & Huber (1982) and Haritonidis (1989). A heated-element heat-transfer shear probe was used in this wind-tunnel investigation, since mass-transfer probes rely on the presence of an aqueous solution.

The principle of operation of a heated-element probe is that the rate of removal of heat from a small heated element, a metal film or wire, mounted on the wall is related to the instantaneous shear stress (or more precisely, the velocity gradient) in the fluid immediately adjacent to the element. Unfortunately, there are several problems inherent in the operation of these probes.

The dynamics of the thermal response of the heated element attenuates the response of the sensor to high-frequency wall shear stress fluctuations. Keith (1990) solved for the dynamic thermal response of a film-type heated-element gauge in a planar boundary layer with an adiabatic substrate:

$$q' = \frac{K_1}{[1+(K_2\,\omega L^{+\frac{2}{3}})^2]^{\frac{1}{2}}}\tau'. \tag{1}$$

This equation shows that the spatially averaged heat flux fluctuation q' corresponding to a wall shear fluctuation of amplitude τ' is a function of the frequency of the shear stress fluctuation ω and the sensor streamwise length L^+. The constants K_1 and K_2 are functions of the mean wall shear stress and heat flux and the thermophysical properties of the fluid. A similar results was obtained by Fortuna & Hanratty (1971) and Mao & Hanratty (1985).

In addition to the heat flux to the fluid flowing over the gauge, heat is also lost by direct conduction to the substrate supporting the heated element. This increases the effective streamwise length of the heated-element gauge L^+ in equation (1), since the thermal boundary layer starts to develop further upstream of the element. Because of the thicker thermal boundary layer resulting at the element, the response of the probe is attenuated even more at high frequencies. Furthermore, at low frequencies, a phenomenon referred to as thermal feedback occurs where the substrate responds to fluctuations in the heat transfer from the element by feeding back thermal waves opposite in phase to the fluctuations (Carslaw & Jaeger 1957). Bellhouse & Schultz (1968) had this problem for their probes for frequencies up to 200 Hz.

At present no analytical or empirical corrections exist for the effects caused by the thermal boundary layer–element–substrate interactions. The most effective way to

minimize these effects is to use a substrate with a low thermal conductivity and to minimize the streamwise length of the heated element. The heated-element shear probe used in these experiments was designed in such a way.

3.2. *Shear probe design and construction*

The heated-element shear probe used in this investigation was the hot-wire-on-the-wall type. The shear-probe substrate was made from low-thermal-conductivity ceramic thermocouple insulation (Omegatite 200, Omega Corp., Stamford, CT). The thermal conductivity of the ceramic was 2.31 $Wm^{-1}K^{-1}$, which is one-quarter that of quartz, the most commonly used substrate material in commercially available hot-film gauges. The cylindrical ceramic piece was 0.114 cm in diameter with two 0.025 cm diameter axial holes separated by 0.025 cm (edge to edge). A jewellers' broach with a 0.0038 cm diameter tip was epoxied in each hole of the ceramic so that it protruded slightly beyond the end of the ceramic. The ceramic was mounted in a cylindrical plug of a low-thermal-conductivity plastic, NORYL EN 265, which was mounted in the test cylinder. The plug was machined so that it had the same radius of curvature as the test cylinder to ensure that it was flush with the test cylinder wall. The NORYL–ceramic–broach assembly was inserted into a hole drilled along the diameter of the test cylinder and was adjusted until the leading edge was within 0.0025 cm ($0.85\nu/u_\tau$) of the surface of the cylinder). According to the investigation carried out by Lefebvre & LaPointe (1986), the flow should not have been affected by a misalignment from flush of this magnitude.

The heated element was made by soft soldering a 2.5 μm diameter Pt–Rh (90/10) alloy wire to the ends of the jewellers' broaches which had been sanded flush with the ceramic surface. The wire was mounted so that it was in contact with the ceramic substrate. Alfredsson *et al.* (1988) recommended a maximum spanwise probe length of $W^+ = 10$–20 for adequate spanwise spatial resolution. However, Shah & Antonia (1987) varied W^+ from 3 to 45 and found no apparent change, within experimental error, in the level of the relative intensity of the wall shear stress fluctuations. In this investigation, the length of the shear-probe wise was 0.0254 cm, corresponding to $W^+ = 9$ and a length-to-diameter ratio of $W/d = 100$. The streamwise length of the heated element was $L^+ = 0.1$, only $\frac{1}{50}$th that of commercial hot-film gauges such as TSI Model 1268W. More details on the shear-probe construction can be found in Wietrzak (1992).

3.3. *Shear-probe frequency response*

Keith's (1990) solution for the dynamic response of a heated film mounted on an adiabatic substrate can be used to estimate the high-frequency limit where the sensor response is affected by attenuation. Since the thermal boundary layer starts to develop upstream of the heated element owing to heat conduction to the substrate, the effective length of the heated element must be estimated and used in place of L^+ in equation (1). The effective length, L_e, is given by Spence & Brown (1968) as

$$L_e^+ = \frac{1}{Pr^{\frac{1}{3}}}\left(\frac{\bar{E}^2}{0.807RWk\,\Delta T}\right)^{\frac{3}{2}}, \tag{2}$$

where Pr and k are the Prandtl number and thermal conductivity of the flow medium, $\bar{E}$ is the average voltage drop across the heated element of resistance R, and ΔT is the temperature difference between heated element and ambient determined from the overheat ratio. Equation (2) overestimates L_e because part of the heat generated, $\bar{E}^2/R$, by the heated element is conducted to the substrate. Using (2), $L_e^+ = 11$. L_e was assumed to be distributed symmetrically about the heated element. Since only the

region upstream of the heated element influences the development of the thermal boundary layer and, hence, on the sensitivity of the probe, $\frac{1}{2}L_e$ was used in determining the upper frequency limit of the shear probe.

Equation (1) requires that the thermal boundary layer lie within the viscous sublayer at the heated-element probe. The thermal boundary layer thickness at the end of the actual heated element was $\delta_t^+ = 5.8$ based on an expression given by Ling (1963). Willmarth *et al.* (1976) have shown that the mean velocity profiles of cylindrical and planar boundary layers are nearly identical within the viscous sublayer. Thus, the unsteady analysis for a planar boundary layer by Keith (1990) leading to (1) is assumed to be valid in our cylindrical boundary layer.

Keith (1990) obtained the one-half power frequency, $\omega_{\frac{1}{2}}$, by setting $K_2 \omega L^{+\frac{2}{3}}$ in (1) equal to unity. The amplitude of the heat flux fluctuation at $\omega_{\frac{1}{2}}$ decreases by 29 % (3 dB) from the value that would occur if the probe had the same response at all frequencies as it does at quasi-steady state. For this investigation, with a free-stream velocity of 11 m s^{-1} and $\delta/a = 5.7$, $\omega_{\frac{1}{2}}$ corresponds to a frequency $f_{\frac{1}{2}} = 2600$ Hz. A square-wave test of the anemometer-probe response gave an upper frequency limit of 17 kHz, indicating that the thermal response of the probe limits the overall response of the system.

3.4. *Shear-probe calibration*

The commonly accepted relationship between the anemometer output voltage and the wall shear stress for hot-film probes is

$$\tau^{\frac{1}{3}} = AE^2 + B, \tag{3}$$

where τ and E are the instantaneous wall shear stress and voltage drop and A and B are calibration constants (Haritonidis 1989). However, this relationship is not obeyed for the type of shear probe where a wire mounted on the surface of the substrate serves as the heated element (Shah & Antonia 1987). In this case it is preferable to use a polynomial of the form

$$\tau = c_0 + c_1 E + c_2 E^2 + \ldots \tag{4}$$

relating the instantaneous output voltage and the instantaneous wall shear stress (Haritonidis 1989). For this investigation a third-order polynomial was used. Its time-averaged form, denoted by the overbar, is

$$\bar{\tau} = c_0 + c_1 \bar{E} + c_2(\bar{E}^2 + \overline{e'^2}) + c_3(\bar{E}^3 + 3\bar{E}\overline{e'^2}), \tag{5}$$

where e' is the fluctuating component of the voltage drop such that $E = \bar{E} + e'$. The constants c_0, c_1, c_2 and c_3 were obtained by calibrating the shear probe *in situ* against the mean wall shear stress obtained with a Preston tube in a turbulent cylindrical boundary layer at 5 to 10 different free-stream velocities and using a least-squares fit to (5). Equation (4) was then used to obtain the instantaneous wall shear stress from the acquired voltage data. In order for the measured wall shear stress fluctuations to fall on the calibration curve the calibration range had to cover values 0.3 to 2.8 times the mean wall shear stress that was measured. A similar calibration range was reported by Alfredsson *et al.* (1988) for a planar wall-bounded flow.

The Preston tube used for calibration had an outer diameter of 0.0559 cm ($d^+ = 10$–30 over the calibration range). The inherent weakness in using a Preston tube in cylindrical boundary layers is that the calibration of the Preston tube in a planar boundary layer must be assumed to be valid in a cylindrical boundary layer. This assumption can be confirmed in two ways.

First, using the planar-boundary-layer calibration is permissible if the outer diameter of the Preston tube falls within the region where the cylindrical velocity profile can be approximated by the planar velocity profile within acceptable error. From the results of Willmarth *et al.* (1976), Lueptow *et al.* (1985), and Lueptow (1988) at $d^+ = 30$ and $\delta/a = 5.7$ the mean velocity profile of a cylindrical boundary layer shows only a minor deviation from that of a planar boundary layer.

Second, Willmarth *et al.* (1976) used Preston tubes of several different diameters to measure the mean wall shear stress in a boundary layer on a 1 in. diameter cylinder and concluded that the shear stress obtained with a Preston tube is correct as long as the ratio of the tube diameter to cylinder diameter is less than 0.3 for $\delta/a = 4.1$. in this investigation, the ratio of the Preston tube diameter to cylinder diameter was 0.059, although $\delta/a = 5.7$ was larger than that of Willmarth.

To calibrate the shear probe the opening of the Preston tube was located at the same axial location on the cylinder as the heated element of the shear probe but offset circumferentially by 90°. Data sets sampled at 8.3 kHz for 6 s (50000 points) were taken at 5 to 10 different free-stream velocities. The corresponding differences between pressures at the Preston tube and the static pressures were measured using a differential pressure transducer. The mean wall shear stresses were obtained using the results of Head & Ram (1971). The calibration was repeated after data were taken and the data were discarded if the calibration changed by more than 2%.

4. Results: characteristics of the wall shear stress fluctuations

4.1. *Intensity of wall shear stress fluctuations*

The relative intensity of the wall shear stress fluctuations, $\tau_{rms}/\bar{\tau}$, indicates the level of turbulence near the wall. The values of the $\tau_{rms}/\bar{\tau}$ ratio reported by various investigators range from 0.06 to 0.40 for various wall-bounded flows, although recent careful measurements put the values of the wall shear stress intensity at 0.36 to 0.40 (Alfredsson *et al.* 1988). Many measurements of the quantity are tabulated in table 2 and shown in figure 2 as a function of spanwise resolution of the probe, W^+. The wide variation is attributed to factors such as spanwise spatial averaging, heat loss to the substrate, and the frequency response of the various probes. The probes with a fine wire as the heated element (filled symbols) usually measured higher values of $\tau_{rms}/\bar{\tau}$ in air compared to hot-film probes for the same spanwise resolution. This suggests that attenuation of the probe frequency response is much greater for hot-film probes because of their longer effective length as noted in §3.1. The fluid medium also affects the measurement of the fluctuating wall shear stress. The power transferred to the fluid is smallest for air and greatest for water (Alfredsson *et al.* 1988). This suggests that the importance of heat loss to the substrate is greatest with air and smallest with water, resulting in more attenuation of the wall shear stress signal in air than water. In addition the high-frequency response limit of the probe is inversely related to the Prandtl number of the fluid (Alfredsson *et al.* 1988). As a result, measurements in oil suffer the greatest high-frequency attenuation and measurements in air suffer the least. It is also evident from figure 2 that spanwise averaging reduces $\tau_{rms}/\bar{\tau}$ as W^+ becomes large.

The wall shear stress intensity measured for six different momentum-thickness Reynolds numbers ranging from 2000 to 4060 was $\tau_{rms}/\bar{\tau} = 0.32$. The typical standard deviation in the wall shear stress intensity over 5 to 9 measurements at each Reynolds number was 0.02 and most likely resulted from daily calibration changes, different sensor wires, and minor variations in wind-tunnel conditions over the period of several

Investigator	W^+	$\tau_{rms}/\bar{\tau}$	Measurement technique	Flow type	Flow medium
Alfredsson *et al.* (1988)	17	0.095	hot film	boundary layer	air
	33	0.16	hot film	boundary layer	air
	20	0.39	hot wire on the wall	boundary layer	air
	2	0.2	hot film	channel	oil
	2	0.36	hot film on the wall	channel	oil
	20	0.4	hot film	channel	water
	25	0.35	hot film on the wall	channel	water
Castro *et al.*[a]	20	0.4	pulsed hot wire	boundary layer	air
Chambers *et al.* (1983)	22	0.06	hot film	channel	air
Eckelmann (1974)	4	0.24	hot film	channel	oil
Karlsson *et al.*[a]	*	0.40	laser anemometry	boundary layer	water
Keith & Bennett (1991)	120	0.17	hot film	boundary layer	water
	210	0.13	hot film	boundary layer	water
Kim *et al.* (1987)	*	0.36	numerical simulation	channel	—
Madavan *et al.* (1985)	300	0.22	hot film	boundary layer	water
Mitchell & Hanratty (1966)[b]	38.9	0.32	electrochemical	pipe	water
Popovich (1969)[a]	*	0.38	flash photolysis	channel	water
Shah & Antonia (1987)	6.1	0.23	hot wire on the wall	channel	air
	11.7	0.27	hot wire on the wall	channel	air
	18.2	0.29	hot wire on the wall	channel	air
	25.7	0.29	hot wire on the wall	channel	air
	31.3	0.29	hot wire on the wall	channel	air
	38.7	0.28	hot wire on the wall	channel	air
	45.3	0.27	hot wire on the wall	channel	air
Sreenivasan & Antonia (1977)	62.7	0.25	hot film	channel	air
Thomas[a]	40	0.12	hot film	boundary layer	air
Present study	9	0.32	hot wire on the wall	boundary layer	air

[a] As given in Alfredsson *et al.* (1988).
[b] Values corrected for spatial averaging.
* W^+ cannot be defined so data are not included in figure 2.

TABLE 2. Measurement of $\tau_{rms}/\bar{\tau}$ reported in the literature

weeks. The value of 0.32 is similar to the values for planar wall-bounded flows obtained using a hot-wire-on-the-wall probe shown in figure 2, although it is slightly less than more recent careful measurements (Alfredsson *et al.* 1988). It is difficult to determine the dependence, if any, of $\tau_{rms}/\bar{\tau}$ on the Reynolds number because of the limited velocity range possible in the experimental facility.

4.2. *Probability density distribution of wall shear stress*

The probability density distribution of the instantaneous wall shear stress in the cylindrical boundary layer for $\delta/a = 5.7$ is shown in figure 3. Based on six data sets, the average standard deviation over all the points due to experimental scatter is 0.0117. Although δ/a was varied from 5.5 to 6.0 in this investigation, the probability density curves for the other cases are not shown because they all lie within the experimental error of the $\delta/a = 5.7$ case. A Gaussian distribution and the distribution of the wall shear stress fluctuations in a planar wall-bounded flow are also shown in figure 3 for comparison. The probability density distributions for the planar wall-bounded flow and the cylindrical boundary layer are similar suggesting that transverse curvature does

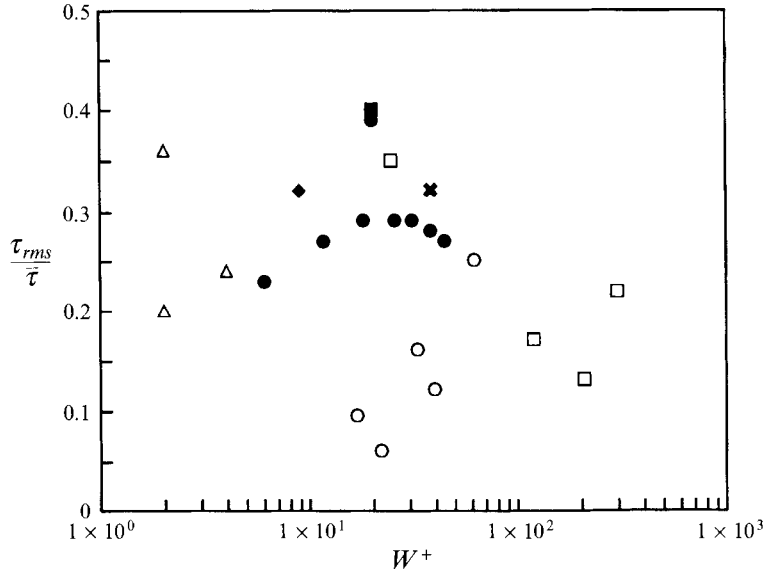

FIGURE 2. Intensity of the wall shear stress fluctuations as a function of probe type for measurements listed in table 2 (open symbols, hot-film; filled symbols, hot wire on the wall) and heated-element spanwise length. Flow medium: ○, air; △, oil; □, water. Here ✖ corresponds to an electrochemical cell in water (Mitchell & Hanratty 1966); ◆, present investigation.

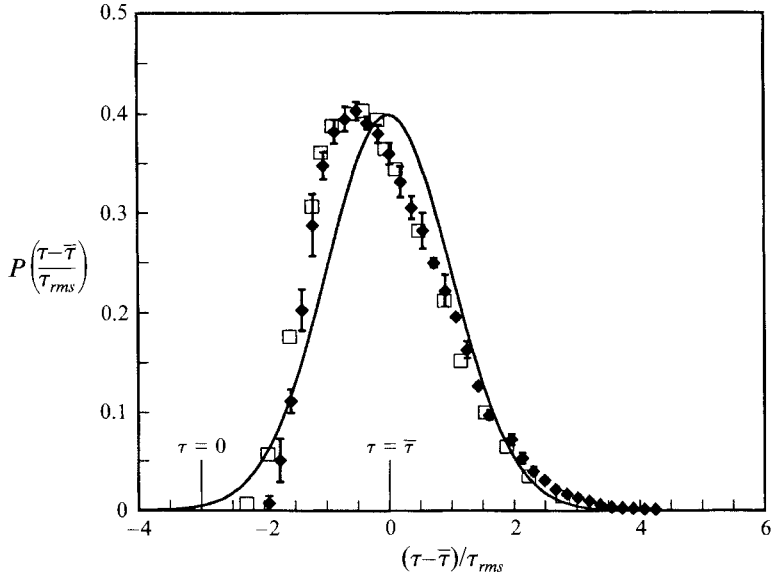

FIGURE 3. Probability density of the wall shear stress fluctuations: ◆, cylindrical boundary layer ($R_\theta = 3050$, $\delta/a = 5.7$, error bars are $\pm\sigma$); □, channel flow, hot-film, $U_0 D/\nu = 6050$ where U_0 is the centreline velocity and D is the channel half-width (Sreenivasan & Antonia 1977); ——, Gaussian distribution.

not affect the turbulent wall shear stress. It is also clear that no flow reversals at the wall ($\tau < 0$) occur in either case.

The skewness, S, and flatness, F, of the wall shear stress obtained in this investigation and by other investigators for planar wall-bounded flows are given in

Investigator	S	F	Flow type
Sreenivasan & Antonia (1977)	0.53	3.1	channel
Kreplin (as given in Eckelmann 1974)	0.75	3.7	channel
Alfredsson *et al.* (1988)	1.00	4.80	channel & boundary layer
Present ($\pm\sigma$ for 6 data sets)	0.80 ± 0.087	3.65 ± 0.274	boundary layer

TABLE 3. Skewness S and flatness F of wall shear stress fluctuations

table 3. The values for the cylindrical boundary layer reported here are similar to those for planar wall-bounded flow. The lack of flow reversals at the wall gives in the probability density distribution a longer positive than negative tail, resulting in a positive skewness. Flatness greater than the Gaussian value of 3.0 results from a longer tail on the positive side in the shear stress distribution than in a Gaussian distribution.

4.3. *Wall shear stress spectrum*

Spectra of the wall shear stress were obtained to determine the effect of the transverse curvature on the frequency distribution of turbulent energy near the wall. The power spectral density function $\Phi(f)$ of the fluctuations of the wall shear stress about its mean is defined such that

$$\tau_{rms}^2 = \int_0^\infty f\Phi(f)\,\mathrm{d}(\ln f), \tag{6}$$

where f is the frequency. Using this form to plot the power spectrum, the energy between any two frequencies is proportional to the area under the curve bounded by those frequencies, so that the relative contribution of each frequency range to the mean-square values is easily evident. The power spectral density function was calculated using a standard fast Fourier transform (Newland 1984) with a rectangular spectral window on 39 data sets consisting of 2^{11} data points each, and then ensemble averaged.

Figure 4 shows the normalized power spectral density non-dimensionalized using inner variables and averaged over six identical measurements in a cylindrical boundary layer. The spectra of the wall shear stress of other wall-bounded flows are also shown in figure 4 for comparison. The ordinate is normalized by τ_{rms}^2 so that the total are under the curve is equal to unity. Deviations from unity of the area under the curve, noted in the caption, suggest errors in the measurement where either a fraction of energy or an excess of energy is included in the plot, or too few points were available to accurately integrate. Non-dimensionalization using outer variables results in similar spectra.

The most noticeable feature of the wall shear stress spectrum appears to be a higher energy content of the planar wall-bounded flows and pipe flow at lower frequencies compared to that of a cylindrical boundary layer. At the higher frequencies, the cylindrical-boundary-layer spectrum contains more energy. This is similar to what Willmarth *et al.* (1970) observed for the spectral density distribution of wall-pressure fluctuations in planar and cylindrical boundary layers. Willmarth's explanation was that the transverse curvature resulted in smaller pressure-producing eddies, thus shifting the spectrum to higher frequencies. In the case of the cylindrical boundary layer, the frequency band where the maximum occurs is centred at $f\nu/u_\tau^2 \approx 1\times10^{-2}$, or $f\delta/U_0 \approx 4\times10^{-1}$, and corresponds to that found by Lueptow & Haritonidis (1987) for

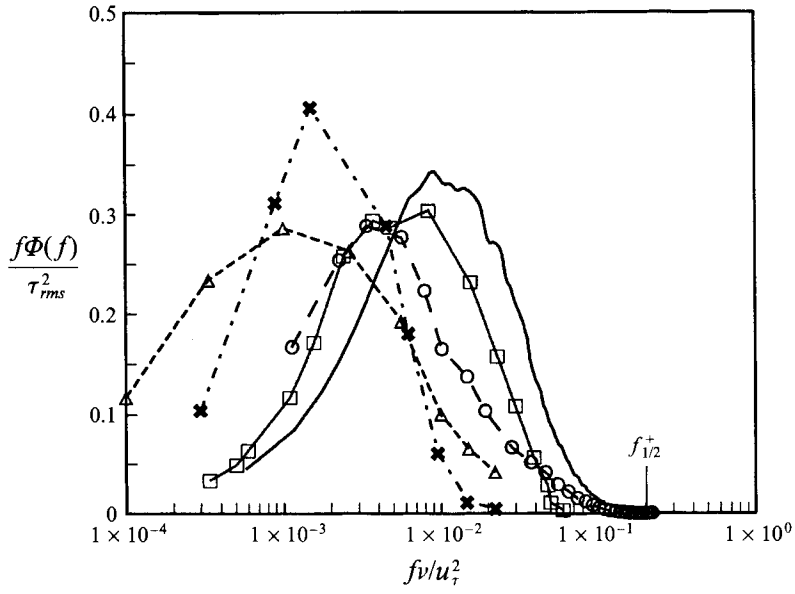

FIGURE 4. Normalized power spectral density: ——, cylindrical boundary layer ($R_\theta = 3050$, $\delta/a = 5.7$); △, planar boundary layer (hot-film, $R_\theta = 10630$, Madavan *et al.* 1985); ✱, pipe flow (electrochemical probe, $\bar{U}d/\nu = 22900$, where d is the pipe diameter, Mitchell & Hanratty 1966); □, channel flow (hot-film, $U_0 D/\nu = 11780$, Sreenivasan & Antonia 1977); ○, planar boundary layer (hot-film, $R_\theta = 8200$, Keith & Bennett 1991). Half-power frequency of shear probe used in this investigation indicated by $f^+_{\frac{1}{2}}$. Area under each curve: ——, 1.0; △ 1.19; ✱, 1.06; □, 0.92; ○, 0.88.

the streamwise velocity spectra in a cylindrical boundary layer. The maximum energy occurring at $f \sim O(U_0/\delta)$ suggests that the structures responsible for most of the wall shear stress fluctuations are large-scale phenomena.

5. Results: event detection

5.1. *VITA and peak event detection*

The VITA technique utilizes short-time variance of the streamwise velocity signal as a measure of the turbulent activity. The short-time variance of the fluctuating component u' of the streamwise velocity u at time t is defined as

$$\mathrm{var}\,(t, T) = \frac{1}{T}\int_{t-\frac{1}{2}T}^{t+\frac{1}{2}T} u'^2(s)\,\mathrm{d}s - \left(\frac{1}{T}\int_{t-\frac{1}{2}T}^{t+\frac{1}{2}T} u'(s)\,\mathrm{d}s\right)^2. \tag{7}$$

T is the averaging time chosen such that it is of the order of the timescale of the phenomenon under study. An event is said to occur when the short-time variance (7) satisfies

$$\mathrm{var}(t, T) > k u^2_{rms}, \tag{8}$$

where k is a chosen threshold level and u^2_{rms} is the long-time averaged variance (Blackwelder & Kaplan 1976). The point midway between the beginning and end of the period that the threshold is exceeded is taken as the reference time for the event.

The peak detection technique detects the occurrence of high-amplitude peaks in the fluctuating components of velocity or wall shear stress signals indicating intense

turbulent events. A peak event is considered to occur when the amplitude of the signal $S(t)$ exceeds kS_{rms}.

In VITA and peak detection, an additional criterion is imposed to distinguish the types of events detected. If at the time of detection, $\partial u'/\partial t > 0$ in VITA or the sign of the peak is positive in peak detection, the event is referred to as a positive event. Negative events have the opposite sign. The ensemble average of the events that exceed the threshold level k is known as the conditional average.

For VITA detection, the number of times (8) is satisfied depends on k and T. Generally, there is not a single value of k where the number of detections is independent of T, although in this investigation a similar frequency of events was detected for a relatively wide range of T when $k = 1$. On this basis, the value of k equal to unity was chosen as the threshold level for VITA. Other investigators such as Johansson & Alfredsson (1982), Alfredsson & Johansson (1984), and Shah & Antonia (1987) have also used a value of $k = 1$ for investigations of planar wall-bounded flows. The positive events are most readily identifiable with the burst–sweep cycle (Blackwelder & Kaplan 1976). Therefore, this analysis concentrates heavily on investigating the conditional averages of those events. At $y^+ = 30$, the greatest number of positive events detected with VITA occurs when $T^+ = 15$ ($k = 1$). This is very similar, within experimental error, to what has been observed by Lueptow & Haritonidis (1987) in a cylindrical boundary layer at comparable y^+ and U_0. Thus, the nominal value of T^+ chosen for use throughout this investigation is 15 viscous time units. Other investigators, such as Johansson & Alfredsson (1982) and Shah & Antonia (1987) have used comparable values of T^+ in planar wall-bounded flows. In all the cases considered here, the threshold level k in peak detection was adjusted to give the same number of events detected with $k = 1$, $T^+ = 15$ in VITA. In this way, events appearing at the same frequency could be compared.

The conditional averages of the positive VITA and peak events at various locations from the wall are shown in figures 5(*a*) and 5(*b*), respectively. Following Blackwelder & Kaplan (1976), the conditional averages of u' and τ' are non-dimensionalized with $k^{\frac{1}{2}}u_{rms}$ and $k^{\frac{1}{2}}\tau_{rms}$, respectively, and are denoted by $\langle\ \rangle^*$. The time coordinate is scaled with the viscous timescale. The most distinct feature of the curves is that for $t^+ < 0$ the deceleration of the fluid at the wall is almost non-existent (figure 5*a*), similar to the results of Chambers, Murphy & McEligot (1983) for flow in a channel. However, as the distance from the wall increases so does the deceleration of the fluid for $t^+ < 0$. In the viscous sublayer the deceleration is small. Further from the wall, the deceleration becomes more pronounced although the peak at $t^+ > 0$ is smaller. Nevertheless, the peak-to-peak amplitude remains the same, about three times the long-time r.m.s. value, regardless of distance from the wall. This behaviour is consistent with what has been observed by Johansson & Alfredsson (1982) for turbulent channel flow.

The conditional average of τ' for $k = 1$, $T^+ \approx 13$ obtained by Shah & Antonia (1987) in duct flow is also shown in figure 5(*a*). It can be compared to our results for $T^+ = 15$ because the conditional averages of τ' for $T^+ \approx 13$–15 in this investigation are nearly identical. Their Reynolds number of 2.11×10^4 based on duct half-width and centreline velocity is comparable to ours of 1.93×10^4 based on δ and U_0. The same type of wall shear stress probes were used in both investigations. From figure 5(*a*), the peak in $\langle\tau'\rangle^*$ in planar wall-bounded flows is 11% smaller than that in the cylindrical boundary layer. Furthermore, the maximum frequency of positive VITA events detected in the cylindrical-boundary-layer case is 20% greater than that obtained by Shah & Antonia (1987). In addition, the averaging time T at which the maximum number of positive events is detected in τ' is 10% larger in the duct-flow case than the

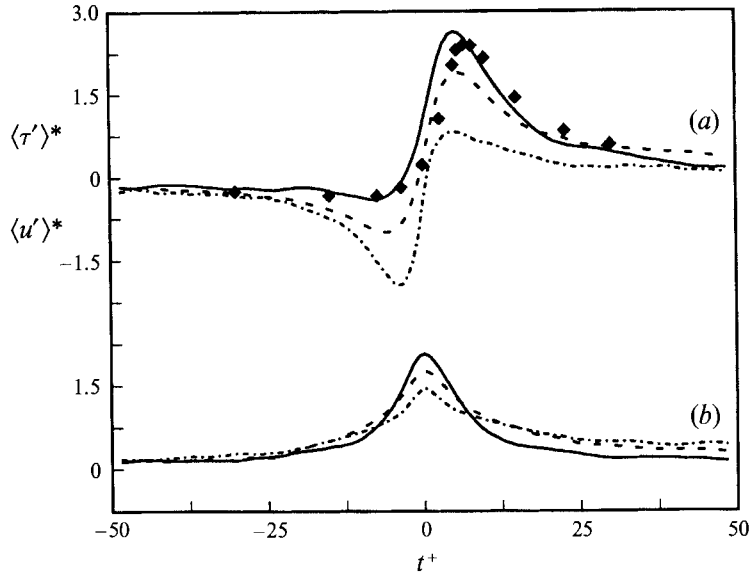

FIGURE 5. Conditional averages of positive events as a function of y^+ equal to: ——, 0 (wall shear stress); ----, 8.41 (velocity); – · –, 39 (velocity). Here: (*a*) VITA detection ($k = 1$, $T^+ = 15$); (*b*) peak detection (same y^+ and number of events as in VITA) ——, $k = 2.86$ (118 events); ----, $k = 2.46$ (111 events); – · –, $k = 1.78$ (219 events); ◆, (wall shear stress for planar wall-bounded flow, $k = 1$, $T^+ = 13$, Shah & Antonia 1987)

cylindrical boundary layer. These results suggest that turbulent events detected at the wall in a cylindrical boundary layer occur more frequently and are of a shorter timescale than in planar wall-bounded flows. A shorter timescale suggests higher frequencies, which is consistent with the power spectra shown in figure 4.

The amplitude of the conditional averages of peak events (figure 5 curve *b*) decreases with increasing distance from the wall. This is similar to what happens in the case of positive VITA events for $t^+ > 0$ (figure 5 curve *a*). The peak also has a narrower base for measurements near the wall indicating that the events are either shorter or not smeared in time as much as events further from the wall. The number of events detected near the wall and at $y^+ = 8.4$ is about half that detected at $y^+ = 39$ for the same detection criteria. This suggests that while there are few events that can overcome the damping effect of the wall, the ones that do overcome it and are detected are very energetic.

5.2. *Conditionally averaged velocity and wall shear stress*

The instantaneous relationship between the wall shear stress and the velocity was investigated by simultaneously measuring both signals. The velocity and shear-probe configurations discussed henceforth refer to the schematic shown in figure 1. In that schematic θ is the angle between probes, Δx is axial displacement between probes, S is arclength at the wall of the cylinder corresponding to angle θ, and y is height of the hot-wire velocity probe above the wall.

Figure 6 shows simultaneous conditional averages of velocity and wall shear stress for configurations where the velocity probe is located directly above the shear probe ($\Delta x = 0$ and $S = 0$) at two different wall-normal locations. The VITA and peak event detection techniques were applied to the velocity signal, and phase-jitter effects were removed from the resulting conditional average of τ'. Phase jitter, a consequence of the

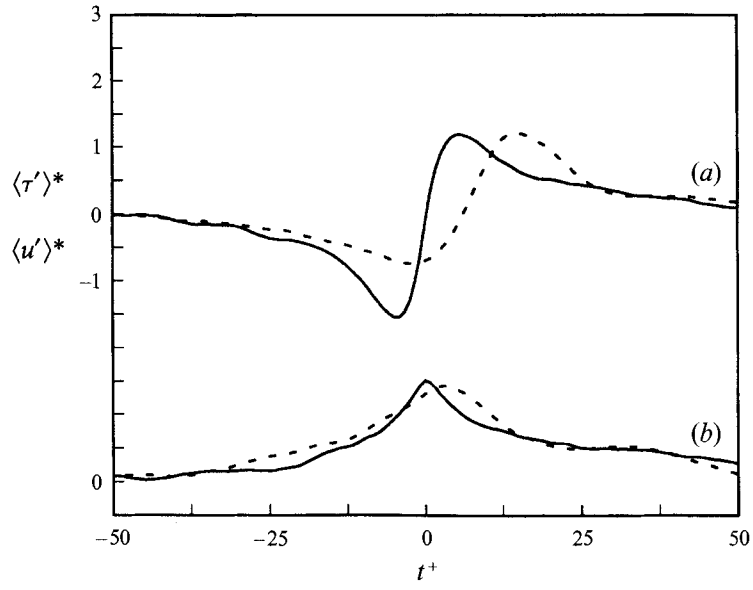

FIGURE 6. Conditional averages of positive events detected using VITA and peak detection techniques on streamwise velocity at $y^+ = 13$. Here ——, $\langle u' \rangle^*$; ----, $\langle \tau' \rangle^*$. (*a*) VITA detection ($k = 1$, $T^+ = 15$, 221 events), (*b*) peak detection ($k = 1.9$, 220 events).

randomness in the passage of the turbulent structures from the detection probe to the non-detection probe, results in some cancellation of coherence that is present, decreasing the magnitude of the conditional average measured at the non-detection probe (Blackwelder 1977). To overcome this problem, the phase information was regained by allowing for changes in the structure using a procedure similar to that implemented by Zilberman, Wygnanski & Kaplan (1977) and Johansson, Her & Haritonidis (1987). In the iterative alignment procedure for both VITA and peak detection, the conditional average with the jitter present is used as a characteristic signature and each realization is cross-correlated with that conditional average over a specified time window. An appropriate time shift is determined by the displacement of the maximum in the cross-correlation. A new conditional average is computed and the procedure is repeated. Using a time window $50\nu/u_\tau^2$ long, similar to that used by Johansson *et al.* (1987), three iterations through the jitter removal algorithm proved sufficient.

It is evident from figure 6 that the velocity probe detects the events ahead of the shear probe. The time delay increases as the velocity probe is displaced further away from the shear probe (not shown). The conditional average of the shear stress is smeared in time. Thomas & Bull (1983) obtained comparable results in a planar boundary layer using a similar velocity/shear probe configuration. They explained the time delay between the detection of the events by the two probes using a model of a structure inclined to the wall in the streamwise direction such that the velocity probe detects the structure ahead of the shear probe. Such coherent structures have been termed 'backs' and are typically inclined at 12° to 25° to the wall (Kline & Robinson, 1990). Using the peak conditional average, it is possible to define a unique time delay between signals. Using the time delay between peaks in figure 6 curve (*b*) and the corresponding result for the velocity probe positioned at $y^+ = 30$ along with a convection velocity of turbulent structures of $U_c \approx 0.51 U_0$ (discussed in §6.1), the average value of the angle of

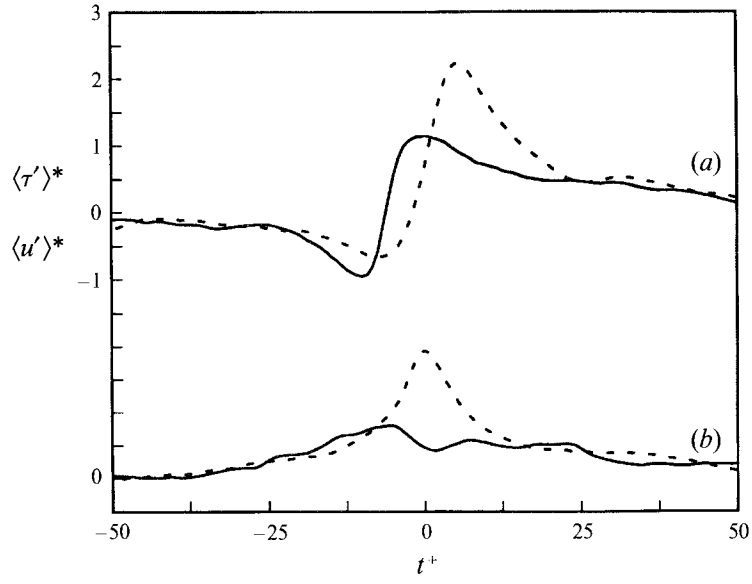

FIGURE 7. Conditional averages of positive events detected using VITA and peak detection techniques on wall shear stress. Here ----, $\langle\tau'\rangle^*$; ——, $\langle u'\rangle^*$ at $y^+ = 13$. (*a*) VITA detection ($k = 1$, $T^+ = 15$, 127 events), (*b*) peak detection ($k = 2.66$, 128 events).

inclination ϕ of the structure was calculated to be 18°. This value of ϕ is the same as that determined by Brown & Thomas (1977) in a planar boundary layer from long-time cross-correlations of the velocity and wall shear stress signals.

In order to investigate the bidirectionality of the phenomenon observed in figure 6, the VITA and peak event detection techniques were applied to the wall shear stress, and jitter effects were removed from the velocity signal. The results are shown in figure 7. The conditional average of VITA events, figure 7 curve (*a*), have a similar character to those in figure 6 curve (*a*) except for the amplitudes. That is, the shear layer is detected by the velocity probe ahead of the shear probe, indicating a bidirectionality in the detection of a shear layer. The difference in amplitudes is a consequence of smearing of the structure from the detection probe to the non-detection probe. If a larger k were used, larger-amplitude events that are more energetic would be detected and the smearing would be reduced. The peak events conditional averages, figure 7 curve (*b*), also show some bidirectionality with those in figure 6 curve (*b*). The time delay between peaks is similar at a given wall-normal position. However, the velocity peaks are not as distinct as in figure 6 curve (*b*), even though the peaks in τ' are much more pronounced. This suggests that there is not necessarily a one-to-one correspondence between surges in wall shear stress and surges in velocity. A possible explanation is that the constraint imposed by the wall on wall-normal motion is most strongly felt only *very near* the wall because of the cylindrical geometry. This could result in a high-amplitude τ' as fluid sweeps toward the wall from the outer region of the boundary layer, but a corresponding surge in streamwise velocity need not be detected by a velocity probe located further away from the wall because the sweep can wash over the cylinder.

The spanwise relationship between turbulent structures was investigated by offsetting the velocity probe from the shear probe in the circumferential direction. Figure 8 curves (*a–c*) shows the conditional averages for $S^+ = 0$, 55, and 100, respectively (see

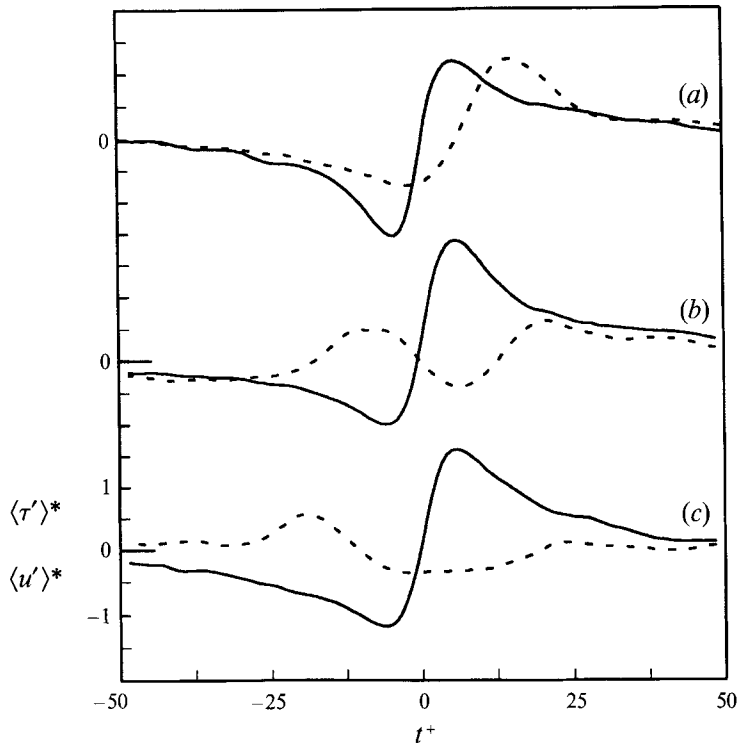

FIGURE 8. Conditional averages of positive events based on VITA detection on streamwise velocity ($k = 1$, $T^+ = 15$). Here ——, $\langle u' \rangle^*$; ----, $\langle \tau' \rangle^*$. (*a*) $y^+ = 13$, $S^+ = 0$, $\Delta x^+ = 0$ (221 events); (*b*) $y^+ = 8$, $S^+ = 55$, $\Delta x^+ = 0$ (111 events); (*c*) $y^+ = 8$, $S^+ = 100$, $\Delta x^+ = 0$ (120 events).

figure 1 for a definition of S^+) corresponding to zero, half and one low-speed streak spacing, which is about $100\nu/u_\tau$ (Lueptow & Jackson 1991). A positive VITA event detection technique was applied on the velocity signal and jitter was removed from the conditional average of the wall shear stress.

The low-speed streaks, thought to be a precursor to the burst-sweep cycle, are separated by regions with a higher fluid velocity. Thus, for an offset of $S^+ = 55$ (shown in figure 8 curve *b*) when the velocity probe detects low-speed fluid for $t^+ < 0$, the shear probe detects high-speed fluid. For $t^+ > 0$, the rapid acceleration, which is believed to be caused by the sweep terminating the burst–sweep cycle, is evident in the conditional average of the velocity. The wall shear stress pattern shows a deceleration for $t^+ > 0$ followed by an acceleration. If that acceleration at the shear probe is caused by the sweep detected at the velocity probe, then the sweep has a circumferential span of at least $55\nu/u_\tau$. The results of Shah & Antonia (1987) lend credibility to this hypothesis. They observed independence of $\tau_{rms}/\bar{\tau}$ using shear probes with spanwise lengths of about $6\nu/u_\tau$ to $45\nu/u_\tau$. Their argument was that the viscous sublayer, according to Cantwell (1981), is dominated by sweeps that have a larger spanwise width than ejections. The delay between the peak in the acceleration of the velocity and that of the wall shear stress for $t^+ > 0$ is consistent with the idea of the inclined structure discussed earlier.

Blackwelder & Eckelmann (1979) used velocity/shear probe configurations similar to those used in this investigation in a channel flow. In their results, reported for a spanwise offset between probes of $6\nu/u_\tau$ to $60\nu/u_\tau$, a positive peak occurs in the

conditional averages of τ' at $-10 < t^+ < 12$ for every spanwise offset greater than $20\nu/u_\tau$. Although Blackwelder & Eckelmann's results do not show the presence of two humps in $\langle\tau'\rangle^*$ like those in figure 8 curve (*b*), no mention is made in their report of corrections for jitter effects. Based on the tests made during this investigation, the peaks and valleys in their conditional averages of τ' may shift and become sharper if jitter is removed. Thus, it cannot be concluded with certainty whether the turbulence mechanisms in planar and cylindrical boundary layers differ significantly.

A circumferential offset of the velocity probe by $100\nu/u_\tau$ in the cylindrical boundary layer results in the conditional averages shown in figure 8 curve (*c*). The peak that occurs in the wall shear stress for $t^+ > 0$ is barely evident, indicating that the sweeping motion is too far away to be detected by the shear probe. The first hump in $\langle\tau'\rangle^*$ remains, indicating that the event is still detected by both probes in spite of their spanwise separation.

6. Results: long-time results

6.1. *Cross-correlations*

The degree to which two signals are related to each other in the time domain can be determined from the correlation coefficient. The long-time correlation coefficient between the velocity and the wall shear stress is defined as

$$R_{u'\tau'}(t) = \overline{u'(\zeta)\tau'(\zeta+t)}/u_{rms}\tau_{rms}, \tag{9}$$

where the overbar denotes a time average and t is the time delay between the signals. The correlation coefficients were calculated using the discrete Fourier transform as described in Newland (1984).

Figure 9 shows the correlations between the velocity and the wall shear stress when the velocity probe is located directly above the shear probe for increasing distance from the wall. Note that the magnitude of $R_{u'\tau'}$ at $t = 0$ is nearly unity near the wall suggesting a very strong correlation. The magnitude of the correlations decreases as the velocity probe is moved farther from the shear probe. The lag time corresponding to the peak value of $R_{u'\tau'}$ increases with distance from the wall, indicating that the structure responsible for the correlation reaches the velocity probe before it reaches the wall shear stress probe. That is, the structure is inclined to the wall in the streamwise direction. Even at a large y^+ of 800 ($y/\delta = 0.9$) there is still a measurable degree of correlation between the two signals. This suggests that the size of the structure is probably on the order of the boundary-layer thickness. The results obtained by Brown & Thomas (1977) and Rajagopalan & Antonia (1979) for planar wall-bounded flows are qualitatively similar to those in figure 9.

The velocity probe was subsequently displaced from the shear probe in the streamwise direction to $\Delta x^+ = 344$ ($\Delta x/\delta = 0.37$, $S^+ = 0$). Since the thermal wake of the shear probe interferes with velocity measurements close to the wall no measurements could be made for $y^+ < 84$. The trend of the correlations is similar to that shown in figure 9. In fact, the maximum magnitude of $R_{u'\tau'}$ is about the same for $\Delta x^+ = 0$ and $\Delta x^+ = 344$ at a similar y^+, suggesting that the structure responsible for the correlations in figure 9 does not weaken substantially as it moves in the streamwise direction. This trend continues for axial displacements as large as $\Delta x^+ = 1002$ (Wietrzak 1992).

For the velocity probe at a wall-normal position of $y^+ = 103$ and a streamwise position of $\Delta x^+ = 344$ downstream of the wall shear stress probe, the lag time for the

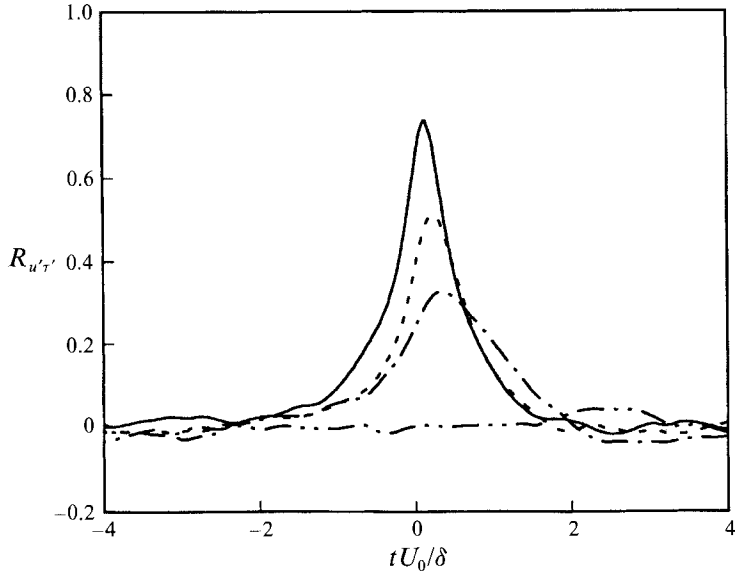

FIGURE 9. Cross-correlation coefficient $R_{u'\tau'}$ for velocity and wall shear stress. Velocity probe is located at $S^+ = 0$, $\Delta x^+ = 0$, and ——, $y^+ = 13$; ---, $y^+ = 30$; – · –, $y^+ = 72$; – · · –, $y^+ = 800$.

maximum correlation is $t \approx 0$. This means that both probes detect the turbulent structure simultaneously. Using a method similar to that used by Brown & Thomas (1977) for a planar wall-bounded flow, the angle of inclination of the structure was found to be $\phi = 17°$. The similarity between this angle for the cylindrical boundary layer and $\phi = 18°$ for a planar boundary layer (Brown & Thomas 1977) suggests that the large-scale structures, with the angle of inclination in the streamwise–wall-normal plane, are similar in the two flows. Furthermore, the average value of the angle of inclination for the cylindrical boundary layer based on time delay between peaks (figure curve 6*b*) is 18°. This suggests that the coherent turbulent structure is a 'back' (Kline & Robinson 1990) and indicates that there is a close relationship between the large-scale structures and the intense turbulent activity occurring near the wall as was suggested by Brown & Thomas (1977) and Thomas & Bull (1983).

The convection velocity of the turbulent structure, U_c, can be estimated using the information from figure 9. Because of the wall-normal spacing of the shear stress probe and the velocity probe, this convection velocity refers to the motion of large-scale inclined structures, not to the convection of the turbulent field. Defining the location of the velocity probe directly above the shear probe as y_u, and the time when the peak in $R_{u'\tau'}$ occurs as t_s, the convection velocity is given by $U_c = y_u/(t_s \tan\phi)$. Using the value of $\phi = 17°$, $U_c/U_0 = 0.51$ at $y^+ = 30$ and $U_c/U_0 = 0.79$ at $y^+ = 72$. The delay time at $y_u^+ = 13$ was not used because the assumption of constant ϕ may not be valid in the region very near the wall (Rajagopalan & Antonia 1979).

Rajagopalan & Antonia (1979) used two hot-film probes separated by 0.98 cm in the streamwise direction to determine U_c/U_0. They found that U_c/U_0 increases from 0.46 at $R_d = 2.2 \times 10^4$ to 0.62 for $R_d > 3.5 \times 10^4$, where R_d is the Reynolds number based on duct half-width and centreline velocity. Brown & Thomas (1977) determined that the convection velocity of the large-scale turbulent structure ranges from $U_c/U_0 = 0.65$ at $y^+ = 170$ to 0.75 at $y/\delta = 0.75$. Thus, the convection velocity measured in this investigation is similar to that measured in planar wall-bounded flows.

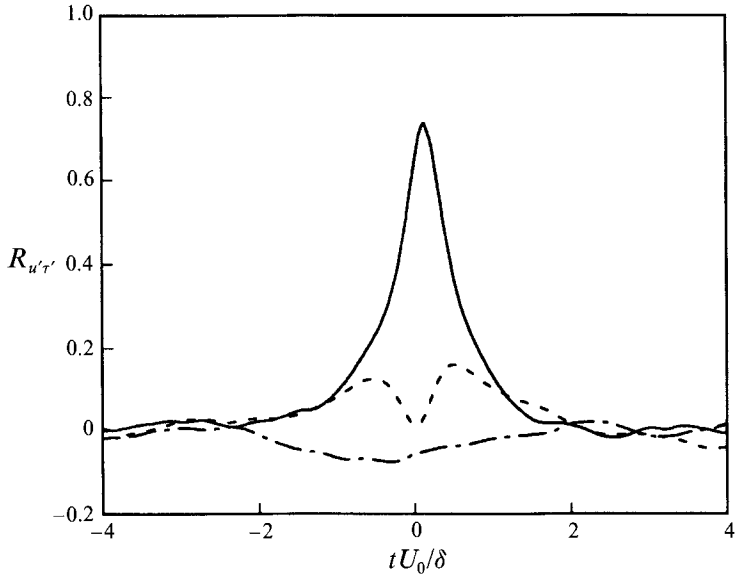

FIGURE 10. Cross-correlation coefficient $R_{u'\tau'}$ for velocity and wall shear stress. Velocity probe is located at ——, $y^+ = 13$, $S^+ = 0$, $\Delta x^+ = 0$; ---, $y^+ = 8.4$, $S^+ = 55$, $\Delta x^+ = 0$; – · –, $y^+ = 8.4$, $S^+ = 100$, $\Delta x^+ = 0$.

Offsetting the velocity probe from the shear probe in the spanwise direction allows the study of the transverse extent of the turbulent structures. Figure 10 shows correlations where the offset positions of the velocity probe were arclengths on the cylinder wall, S^+, of 0, 55, and 100 viscous lengths, corresponding to zero, half, and one low-speed streak spacing. The most striking feature of the correlations is the double peak that occurs in the correlation curve corresponding to $S^+ = 55$. Apparently there are instances when a turbulence structure is detected by the velocity probe ahead of the shear probe and vice versa. This indicates that the leading edge of the structure is at an angle to the axis of the cylinder, or is yawed in the spanwise direction. At $S^+ = 100$, a double peak may be evident at $tU_0/\delta \approx \pm 2.5$, although this is at the noise level of the correlation and may not be significant. Nevertheless, a negative correlation exists between the velocity and the wall shear stress. Kreplin & Eckelmann (1979) also observed that signals from shear probes with a spanwise offset of $100\nu/u_\tau$ are negatively correlated in planar wall-bounded flows. A double peak also appears at $S^+ = 55$ when $y^+ = 39$, although the negative correlation at $S^+ = 100$ disappears at this wall-normal location. These results suggest that the spanwise lengthscale of the turbulent structure responsible for the double peak is greater than $55\nu/u_\tau$ and less than $100\nu/u_\tau$.

In order to investigate the double-peak phenomenon further, a shear probe was constructed that could measure the wall shear stress simultaneously at two points in the spanwise direction. The probe is of the type described in §3.2, with the exception that two heated element/ceramic assemblies were mounted side by side. The heated elements were 3.81×10^{-4} m long ($W^+ = 12.74$ at $U_0 = 11$ m s^{-1}). The distance from centre to centre of the heated elements was 1.02×10^{-3} m ($l^+ = 34$ at $U_0 = 11$ m s^{-1}). The dimensionless length of the heated elements and the distance separating them was adjusted by varying the free-stream velocity to change the value of the friction velocity used in non-dimensionalization.

The cross-correlation curves of the data taken with the double shear probe are shown in figure 11, where τ_1' and τ_2' refer to the shear stress measured by each probes.

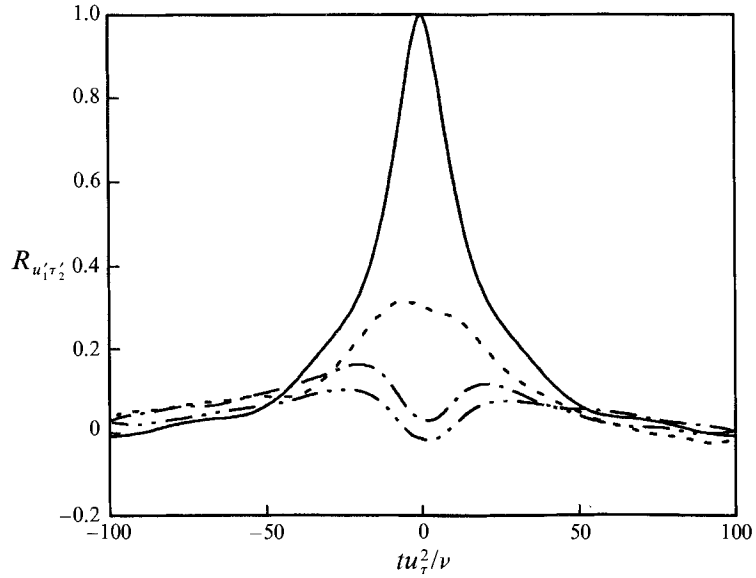

FIGURE 11. Cross-correlation coefficient $R_{\tau'_1\tau'_2}$ for double shear probe; ——, $l^+ = 0$; ---, $l^+ = 21$; – · –, $l^+ = 34$; – · · –, $l^+ = 46$.

The slight asymmetry in the correlations may be due to a 1.6% difference between values of τ_{rms} measured by the two shear probes. The distance from the centre to centre of the heated elements was varied from $l^+ = 0$–46. A length of $l^+ = 0$ corresponds to correlating a signal with itself. The double peak appears in the correlations as the probes are spaced further apart. The maxima of the double peaks in figure 11 occur at greater t^+ as the distance between the probes increases, supporting the idea of a structure yawed relative to the axis of the cylinder. However, the maxima of the double peaks using an outer scaling for time occur at the same tU_0/δ, suggesting that the double hump is not related to a near-wall structure such as streaks.

A sketch of two possible structures that could be responsible for the double peak in figures 10 and 11 is shown in figure 12. One possibility is an arrowhead type structure. Depending on the location of the structure in the spanwise direction relative to the probes, either probe is equally likely to detect it first. Another possibility is that the structure has just one inclined edge, with the angle of inclination being equally probable in either direction. Occurrences of both structures are also possible. The angle of inclination, β, was estimated based on the convection velocity $U_c/U_0 = 0.51$, the spanwise separation of the heated elements of the double shear probe, and the lag time for the peaks in figure 11. The yaw angle is estimated to be $\beta = 81°$ for both $l^+ = 34$ and $l^+ = 46$. Based on the results of figure 10, the span of the inclined structure would be greater than $55\nu/u_\tau$ and less than $100\nu/u_\tau$, as discussed above. An arrowhead-type structure would be twice as wide. Using the yaw angle of 81°, an estimate of the maximum axial length of the structure so that the width does not exceed $100\nu/u_\tau$ is between $347\nu/u_\tau$ (0.39δ) and $630\nu/u_\tau$ (0.70δ).

Simultaneous measurements of the wall shear stress in planar wall-bounded flows using multiple shear stress probes separated by a spanwise distance have been made by Mitchell & Hanratty (1966), Blackwelder & Eckelmann (1979), Kreplin & Eckelmann (1979), Hogenes & Hanratty (1982), and Nikolaides, Lau & Hanratty (1983). However, the only investigators to show the cross-correlation curves between the signals from the shear probes are Kreplin & Eckelmann (1979). In their investigation they varied the

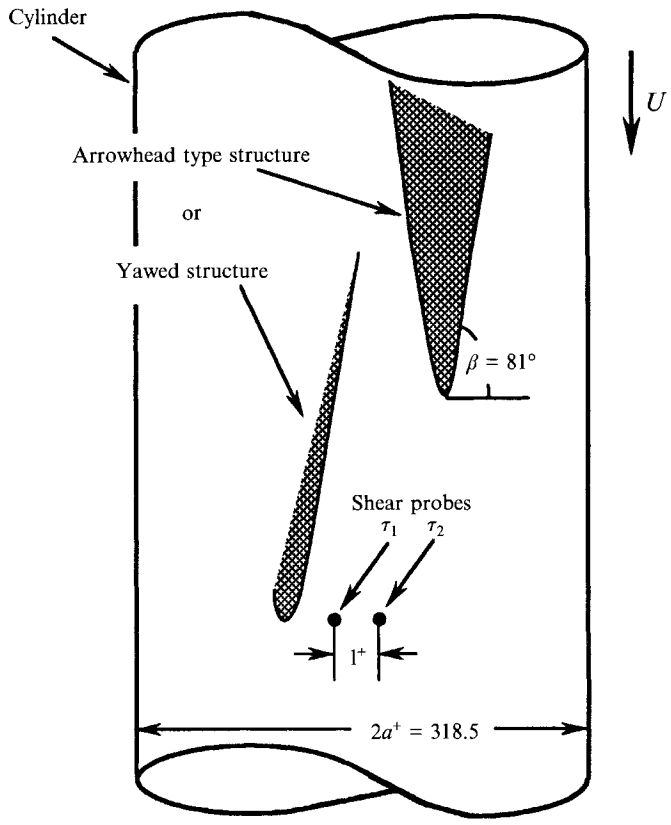

FIGURE 12. Schematic of possible transverse turbulent structures responsible for double peak in the cross-correlations.

distance between shear probes in the range $12.6 \leqslant l^+ \leqslant 105$. The correlation curve for $l^+ = 12.6$ has a maximum at $t = 0$ and is symmetric, as are the correlation curves at the other separation distances. Kreplin & Eckelmann (1979) neither show nor mention the presence of a double peak in their correlation curves. It appears that the inclined structures hypothesized in figure 12 for the boundary layer on a cylinder are not present in planar wall-bounded flows.

Two causes of the inclined structures in the cylindrical boundary layer are possible. First, Lueptow & Haritonidis (1987) observed in their flow visualization experiments that large-scale structures move freely in the boundary layer and can pass from one side of the cylinder to the other. Thus, a large-scale structure can bump into the cylinder and wash across it. Second, the sweeping motion during the burst–sweep cycle could have a similar effect. In either case, the fluid structure approaching the wall would split with one part passing around each side of the cylinder as each part is carried downstream. The resulting structures could be similar to those proposed in figure 12. However, based on figure 8 it was hypothesized that the width of the sweep during the burst–sweep cycle is approximately $55\nu/u_\tau$–$100\nu/u_\tau$ in this investigation. From figure 10 the turbulent structure near the wall responsible for the double peaks in the correlation also appears to be between $55\nu/u_\tau$–$100\nu/u_\tau$ wide. Thus, it is possible that the structures proposed in figure 12 are initiated during the burst–sweep cycle.

The limit on the distance from the wall for which the double peaks in the correlations occur was investigated by positioning the velocity and shear probes at a given spanwise

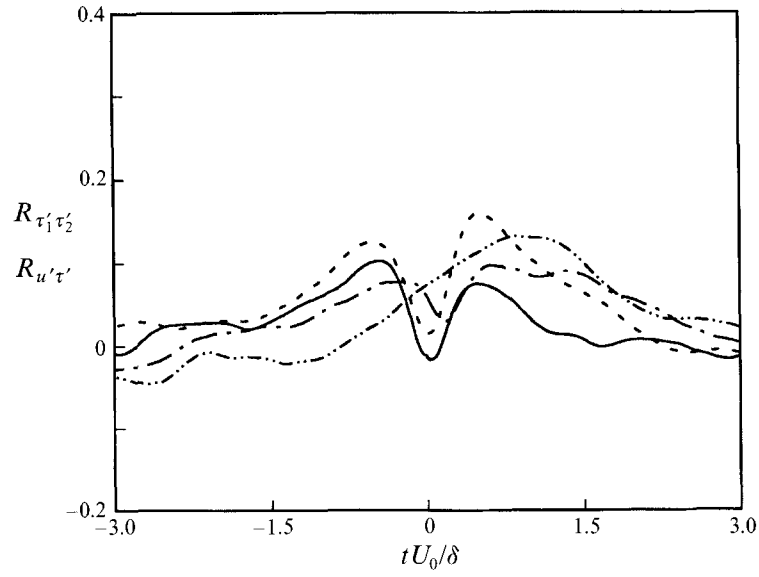

FIGURE 13. Cross-correlation coefficient $R_{u'\tau'}$ for velocity and wall shear stress. Velocity probe is located at: ---, $y^+ = 8.4$, $S^+ = 55$, $\Delta x^+ = 0$; – · –, $y^+ = 39$, $S^+ = 55$, $\Delta x^+ = 0$; – · · –, $y^+ = 210$, $S^+ = 55$, $\Delta x^+ = 0$; ——, $R_{\tau_1'\tau_2'}$ with $l^+ = 46$.

separation and varying the height of the velocity probe above the wall. The variation of the cross-correlation curves with increasing y^+ is shown in figure 13. In addition, $R_{\tau_1'\tau_2'}$ for $l^+ = 46$ (from figure 11) was plotted in figure 13 to give a representative picture of the correlation at the wall. The double peak in the correlation gradually disappears with increasing distance from the wall. At $y^+ = 210$ the double peak is gone, and it has been replaced by a positive correlation. The positive correlation is consistent with the passage of a large-scale coherent structure inclined to the wall.

6.2. *Coherence*

The extent to which two signals are linearly related in the frequency domain can be determined from the coherence function. For simultaneously measured velocity and wall shear stress, the coherence function, $\gamma^2_{u'\tau'}(f)$, is defined as

$$\gamma^2_{u'\tau'}(f) = \frac{|G_{u'\tau'}(f)|^2}{G_{u'u'}(f)\,G_{\tau'\tau'}(f)}, \tag{10}$$

where $G_{u'\tau'}(f)$ is the cross-spectral density function and $G_{u'u'}(f)$ and $G_{\tau'\tau'}(f)$ are the auto-spectral density functions of the velocity and the wall shear stress, respectively (Bendat & Piersol 1986).

The coherence function for the case of the velocity probe located directly above the shear probe is shown in figure 14. Included in figure 14 is a plot of the spectral density distribution for τ' and u' presented in the same format as figure 4. The maximum value of $\gamma^2_{u'\tau'}$ is highest for the case when the velocity probe is closest to the wall at $y^+ = 13$. Its maximum is equal to 0.72, and the high degree of coherence between the two signals is consistent with the fact that in the viscous sublayer u' is proportional to τ'. As the velocity probe is displaced further away from the wall, the magnitude of $\gamma^2_{u'\tau'}$ decreases until it reaches almost zero at $y^+ = 800$. A qualitatively similar trend has been observed by Rajagopalan & Antonia (1979) in a duct flow.

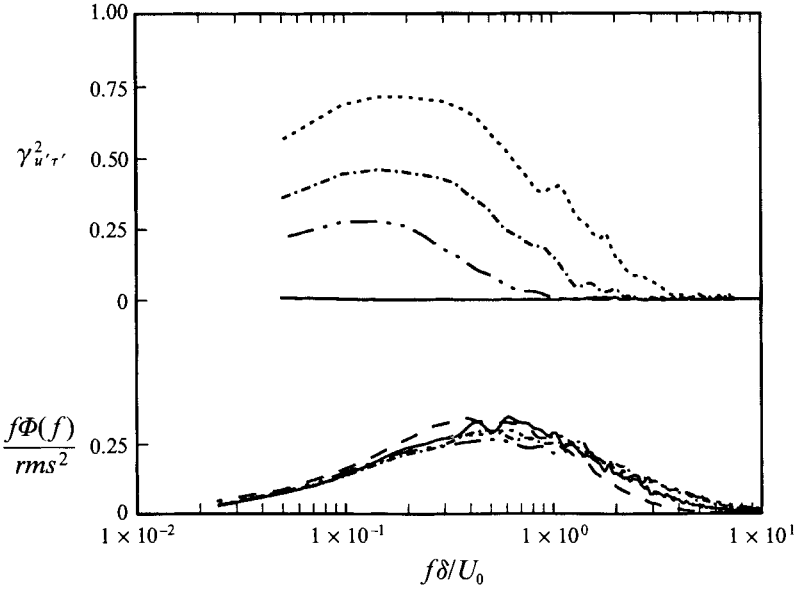

FIGURE 14. Coherence function $\gamma^2_{u'\tau'}$ and power spectral density Φ of velocity and wall shear stress. Velocity probe is located at $S^+ = 0$, $\Delta x^+ = 0$, with y^+ equal to: ---, 13; – · –, 30; – · · –, 72; ——, 800, ——, spectral density of wall shear stress.

From figure 14, it is evident that the peak value of $\gamma^2_{u'\tau'}$ shifts to lower frequencies as the velocity probe is displaced from the shear probe. This can be explained by noting that both probes will detect the same structure only if its lengthscale is larger than the distance separating them. A larger lengthscale implies lower characteristic frequency which leads to a shift of the maximum coherence to a lower frequency band. Perhaps even more important is the small level of coherence for high-frequency components of $f\delta/U_0 > 1$. The peaks in the plots of $\gamma^2_{u'\tau'}$ shown in figure 14 occur in the frequency band centred at $f\delta/U_0 \approx 0.15$. The spectra of τ' and u' have peaks centred at a higher frequency of $f\delta/U_0 \approx 0.60$. Thus, maximum coherence occurs at a frequency where energy is much less than in the τ' or u' spectra. This means that only low-frequency energy is coherent and the high-frequency scales are not related even at very close probe spacing.

The coherence for the cases of the velocity probe being displaced from the shear probe in the spanwise direction is shown in figure 15. The coherence for one-half streak spacing has a double hump, while for zero and one streak spacing there is only one hump. This corresponds to the appearance of a double peak in the cross-correlations for these configurations plotted in figure 10. The double peak in the cross-correlations that occurs when the velocity probe and shear probe are displaced from each other by half a streak spacing occurs at a delay time corresponding to $f\delta/U_0 \approx 2$. This frequency is of the same order as $f\delta/U_0 \approx 1$ for the appearance of the second hump in the coherence for one-half streak spacing. The lower-frequency hump for one-half streak spacing is in the range of frequencies that was related to the inclined structure in figure 14. Thus, the first hump for half-streak spacing between probes at $f\delta/U_0 \approx 0.15$ appears to correspond to the large-scale structure inclined in the streamwise direction. The second hump at $f\delta/U_0 \approx 1$ appears to correspond to the transverse structure yawed relative to the cylinder axis. Similar behaviour is observed in measurements made with the double shear probe (Wietrzak 1992).

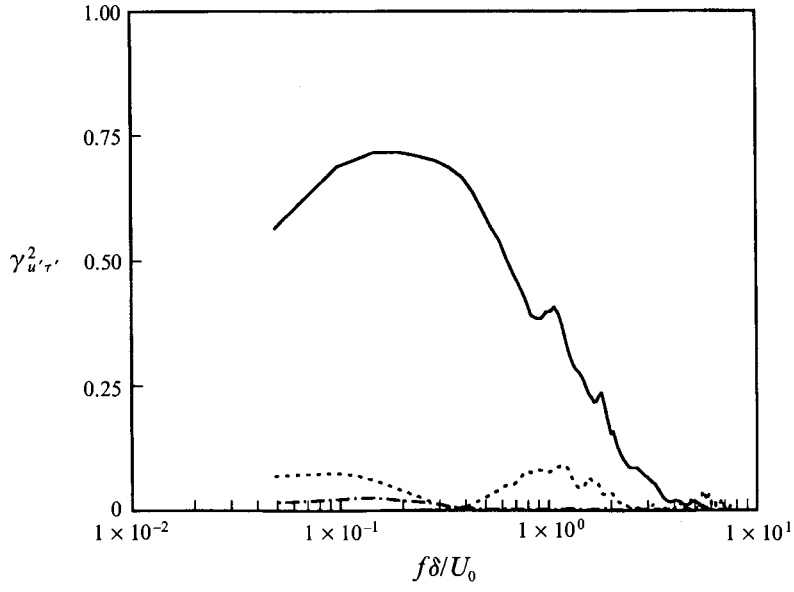

FIGURE 15. Coherence function $\gamma^2_{u'\tau'}$ for velocity and wall shear stress. Velocity probe is located at: ——, $y^+ = 13$, $S^+ = 0$, $\Delta x^+ = 0$; ---, $y^+ = 8.4$, $S^+ = 55$, $\Delta x^+ = 0$; – · –, $y^+ = 8.4$, $S^+ = 100$, $\Delta x^+ = 0$.

7. Conclusions

Our goal has been to determine the effect of transverse curvature on the fluctuating wall shear stress and flow structures in a turbulent boundary layer. The flow parallel to a long slender cylinder with $\delta/a = 5.7$ results in a situation where the effects of transverse curvature are evident. The use of a high-frequency-response hot wire on the wall probe for measuring the streamwise wall shear stress and a hot-wire probe for measuring the streamwise velocity provides a method for relating the structure of the turbulence in the boundary layer above the wall with its signature fluctuating shear stress at the wall.

Very near the wall, the character of the turbulence seems largely unaffected by the transverse curvature. The intensity of wall shear stress fluctuations, $\tau_{rms}/\bar{\tau} = 0.32$, although somewhat low, is within the broad bounds of that for planar wall-bounded flows, and the distribution of the wall shear stress fluctuations is similar to planar wall-bounded flows. The conditionally averaged velocity and wall shear stress traces for VITA and peak detection are similar to those for a flat plate, indicating that the burst–sweep cycle is not substantially altered by transverse curvature, confirming the results of Lueptow & Haritonidis (1987). A relatively strong bidirectionality exists between VITA events detected on the wall shear stress and velocity, indicating that detection on either identifies the same events. The bidirectionality for peak detection is evident although not nearly as strong. The large-scale structures, or backs, that are detected appear to be inclined to the wall at an angle of 18°, similar to the angle found by Brown & Thomas (1977).

Although the transverse curvature does not seem to have a significant effect on the burst–sweep cycle or related structures inclined to the wall, there are two significant effects of transverse curvature on the turbulent boundary layer. First, the energy in the spectrum for the wall shear stress is reduced at low frequencies compared to that for planar wall-bounded flows. Similar results have been obtained for the wall pressure (Willmarth & Yang 1970; Snarski 1992). An explanation of the phenomenon was

presented by Willmarth & Yang based on the result that the convection velocity for pressure-producing eddies is the same in a cylindrical boundary layer as in a planar boundary layer. Since the cylindrical boundary layer has a fuller mean velocity profile, the eddies move faster. To maintain the same convection velocity, the pressure-producing eddies must be smaller. This same effect could reduce the fluctuations in wall shear stress at lower frequencies. However, the energy at high frequencies in a boundary layer on a cylinder must increase, so that $\tau_{rms}/\bar{\tau}$ remains the same as that for a planar boundary layer.

The second effect of transverse curvature is the appearance of the double bump in the cross-correlations when probes are offset in the spanwise direction by one-half streak spacing. The arrowhead or half-arrowhead structure yawed to the axis of the cylinder that could be responsible for this result may be a consequence of fluid washing over the cylinder. The fluid that washes over the cylinder could be related to either the sweep following a burst washing across the cylinder or an eddy of fluid in the outer part of the boundary layer bumping into the cylinder and washing across it. In either case, the coherence indicates that the yawed structure is related to higher frequencies and that the inclined structure is related to lower frequencies.

Based on the results presented here and in previous studies an overall picture of the structure of a thick turbulent boundary layer on a cylinder emerges. As the boundary-layer thickness becomes large compared to the radius of the cylinder, the flow can be thought of as a hybrid between an axisymmetric wake and a boundary layer. The wall continuously converts mean flow energy into turbulent energy with a mechanism that is very similar to that in planar wall-bounded flows. In other words, the transverse curvature has little effect on the flow very near the wall. Away from the wall the cylindrical geometry results in an axisymmetric wake-like flow with the cylinder producing vorticity and turbulence near its centreline. Large structures from the wake-like outer flow or the sweeps following a burst may wash across the cylinder resulting in the yawed structures described in this paper.

This research was supported by the Office of Naval Research under Contract No. N0014-89-J-1439, Mr James A. Fein, Program Manager. Special thanks to Dr David Hurdis, Naval Undersea Warfare Center, New London, CT, for making this research possible.

REFERENCES

ALFREDSSON, P. H. & JOHANSSON, A. V. 1984 Time scales in turbulent channel flow. *Phys. Fluids* **31**, 1974–1981.

ALFREDSSON, P. H., JOHANSSON, A. V., HARITONIDIS, J. H. & ECKELMANN, H. 1988 The fluctuating wall-shear stress and the velocity field in the viscous sublayer. *Phys. Fluids* **31**, 1026–1033.

BELLHOUSE, B. J. & SCHULTZ, D. L. 1968 The measurement of fluctuating skin friction in air with heated thin-film gages. *J. Fluid Mech.* **32**, 675–680.

BENDAT, J. S. & PIERSOL, A. G. 1986 *Random Data: Analysis and Measurement Procedures.* John Wiley & Sons.

BLACKWELDER, R. F. 1977 On the role of phase information in conditional sampling. *Phys. Fluids* **20**, S232–242.

BLACKWELDER, R. F. & ECKELMANN, H. 1979 Streamwise vortices associated with the bursting phenomena. *J. Fluid Mech.* **94**, 577–594.

BLACKWELDER, R. F. & HARITONIDIS, J. H. 1983 Scaling of the bursting frequency in turbulent boundary layers. *J. Fluid Mech.* **132**, 87–103.

BLACKWELDER, R. F. & KAPLAN, R. E. 1976 On the wall structure of the turbulent boundary layer. *J. Fluid Mech.* **76**, 89–112.

BROWN, G. L. & THOMAS, A. S. W. 1977 Large structure in a turbulent boundary layer. *Phys. Fluids.* **20**, S243–S252.

CANTWELL, B. J. 1981 Organized motion in turbulent flow. *Ann. Rev. Fluid Mech.* **13**, 457–515.

CARSLAW, H. S. & JAEGER, J. C. 1957 *Conduction of Heat in Solids.* Oxford University Press.

CHAMBERS, F. W., MURPHY, H. D. & MCELIGOT, D. M. 1983 Laterally converging flow. Part 2. Temporal wall shear stress. *J. Fluid Mech.* **127**, 403–428.

CORINO, E. R. & BRODKEY, R. S. 1969 A visual investigation of the wall region in turbulent flow. *J. Fluid Mech.* **37**, 1–30.

DEWEY, C. F. & HUBER, P. W. 1982 Measurement methods for fluid shear stress. *Annual Summary Report for January 1 to December 31 1980.* Fluid Mech. Laboratory, MIT (March).

ECKELMANN, H. 1974 The structure of the viscous sublayer and the adjacent wall region in a turbulent channel flow. *J. Flow Mech.* **65**, 439–459.

FORTUNA, G. & HANRATTY, T. J. 1971 Frequency response of the boundary layer on wall transfer probes. *Intl J. Heat Mass Transfer* **14**, 1499–1507.

HARITONIDIS, J. H. 1989 The measurement of wall shear stress. In *Advances in Fluid Mechanics Measurements* (ed. M. Gad-el-Hak), pp. 229–262. Springer.

HEAD, M. R. & RAM, V. V. 1971 Simplified presentation of preston tube calibration. *Aeronaut. Q.* **22**, 295–300.

HOGENES, J. H. A. & HANRATTY, T. J. 1982 The use of multiple wall probes to identify coherent flow patterns in the viscous wall region. *J. Fluid Mech.* **124**, 363–390.

JOHANSSON, A. R. & ALFREDSSON, P. H. 1982 On the structure of turbulent channel flow. *J. Fluid Mech.* **22**, 295–314.

JOHANSSON, A. R., HER, J. & HARITONIDIS, J. H. 1987 On the generation of high-amplitude wall-pressure peaks in turbulent boundary layers and spots. *J. Fluid Mech.* **175**, 119–142.

KEITH, W. L. 1990 Spectral measurements of the wall shear stress and wall pressure in a turbulent boundary layer: Theory. *US NUSC Tech. Rep.* 8295.

KEITH, W. L. & BENNETT, J. C. 1991 Low frequency spectra of the wall shear stress and wall pressure in a turbulent boundary layer. *AIAA J.* **29**, 523–530.

KELLY, H. R. 1954 A note on the laminar boundary layer on a circular cylinder in axial incompressible flow. *J. Aero Sci.* **21**, 634.

KIM, H. T., KLINE, S. J. & REYNOLDS, W. C. 1971 The production of turbulence near a smooth wall in a turbulent boundary layer. *J. Fluid Mech.* **50**, 133–160.

KIM, J., MOIN, P. & MOSER, R. 1987 Turbulence statistics in fully developed channel flow at low Reynolds number. *J. Fluid Mech.* **177**, 133–166.

KLINE, S. J., REYNOLDS, W. C., SCHRAUB, F. A. & RUNSTADLER, P. W. 1967 The structure of turbulent boundary layers. *J. Fluid Mech.* **30**, 741–773.

KLINE, S. J. & ROBINSON, S. K. 1990 Quasi-coherent structures in the turbulent boundary layer: Part I. Status report on a community-wide summary of data. In *Near Wall Turbulence: 1988 Zoran Zaric Memorial Conf.* (ed. S. J. Kline & N. H. Afgan), pp. 200–217. Hemisphere.

KREPLIN, H. P. & ECKELMANN, H. 1979 Propagation of perturbations in the viscous sublayer and adjacent wall region. *J. Fluid Mech.* **95**, 305–322.

LEFEBVRE, P. J. & LAPOINTE, K. M. 1986 The effect of mounting position on hot-film wall shear stress sensors. *AIAA*-86-1101. *AIAA/ASME 4th Fluid Mechanics, Plasma Dynamics and Laser Conf., May 12–14, Atlanta, Georgia.*

LING, S. C. 1963 Heat transfer from a small isothermal spanwise strip on an insulated boundary. *Trans. ASME* C: *J. Heat Transfer* **85**, 230–236.

LUEPTOW, R. M. 1988 Turbulent boundary layer on a cylinder in axial flow. *US NUSC Tech. Rep.* 8389.

LUEPTOW, R. M. 1990 Turbulent boundary layer on a cylinder in axial flow. *AIAA J.* **28**, 1705–1706.

LUEPTOW, R. M. & HARITONIDIS, J. H. 1987 The structure of the turbulent boundary layer on a cylinder in axial flow. *Phys. Fluids* **30**, 2993–3005.

LUEPTOW, R. M. & JACKSON, C. P. 1991 Near-wall streaky structure in a turbulent boundary layer on a cylinder. *Phys. Fluids* A **3**, 2822–2824.

LUEPTOW, R. M., LEEHEY, P. & STELLINGER, T. 1985 The thick turbulent boundary layer on a cylinder: mean and fluctuating velocities. *Phys. Fluids* **28**, 3495–3505.

LUXTON, R. E., BULL, M. K. & RAJAGOPALAN, S. 1984 The thick turbulent boundary layer on a long fine cylinder in axial flow. *Aero. J.* **88**, 186–199.

MADAVAN, N. K., DEUTSCH, S. & MERKLE, C. L. 1985 Measurements of local skin friction in a microbubble-modified turbulent boundary layer. *J. Fluid Mech.* **156**, 237–256.

MAO, Z. X. & HANRATTY, T. J. 1985 The use of scalar transport probes to measure wall shear stress in a flow with imposed oscillations. *Exps Fluids* **3**, 129–135.

MITCHELL, J. E. & HANRATTY, T. J. 1966 A study of turbulence at a wall using an electrochemical wall shear-stress meter. *J. Fluid Mech.* **26**, 199–221.

NEWLAND, D. E. 1984 *Random Vibrations and Spectral Analysis*, 2nd edn. Longman.

NIKOLAIDES, C., LAU, K. K. & HANRATTY, T. J. 1983 A study of the spanwise structure of coherent eddies in the viscous wall region. *J. Fluid Mech.* **130**, 91–108.

PATEL, V. C. 1965 Calibration of the Preston tube and limitations on its use in pressure gradients. *J. Fluid Mech.* **23**, 185–208.

POPOVICH, A. T. 1969 Statistical analysis of fluid flow fluctuations in the viscous layer near a solid wall. *Ind. Engng Chem. Fundam.* **8**, 609–614.

RAJAGOPALAN, S. & ANTONIA, R. A. 1979 Some properties of the large structure in a fully developed turbulent duct flow. *Phys. Fluids* **22**, 614–622.

RICHMOND, R. L. 1957 Experimental investigation of thick axially symmetric boundary layers on cylinders at subsonic and hypersonic speeds. *Hypersonic Res. Proj. Memo.* 39. California Institute of Technology.

ROBINSON, S. K. 1990 A review of vortex structures and associated coherent motions in turbulent boundary layers. In *Structure of Turbulence and Drag Reduction IUTAM Symp. Zurich, Switzerland 1990* (ed. A. Gyr), pp. 23–50. Springer.

SHAH, D. A. & ANTONIA, R. A. 1987 Scaling of wall shear stress fluctuations in a turbulent duct flow. *AIAA. J.* **25**, 22–29.

SHAH, D. A. & ANTONIA, R. A. 1989 Scaling of the bursting period in turbulent boundary layer and duct flows. *Phys. Fluids* A **1**, 318–325.

SNARSKI, S. R. 1992 Relationship between the fluctuating wall pressure and the turbulent structure of a boundary layer on a cylinder in axial flow. PhD thesis, Northwestern University, Dept. of Mech. Engng.

SPENCE, D. A. & BROWN, G. L. 1968 Heat transfer to a quadratic profile. *J. Fluid Mech.* **33**, 753–773.

SREENIVASAN, K. R. & ANTONIA, R. A. 1977 Properties of wall shear stress fluctuations in a turbulent duct flow. *Trans. ASME* E: *J. Appl. Mech.* **44**, 389–395.

THOMAS, A. S. W. & BULL, M. K. 1983 On the role of wall-pressure fluctuations in deterministic motions in the turbulent boundary layer. *J. Fluid Mech.* **128**, 283–322.

WIETRZAK, A. 1992 The fluctuating wall shear stress in the turbulent boundary layer on a cylinder in axial flow. PhD thesis, Northwestern University, Dept. of Mech. Engng.

WILLMARTH, W. W., WINKEL, R. E., SHARMA, L. K. & BOGAR, T. J. 1976 Axially symmetric turbulent boundary on cylinders: mean velocity profiles and wall pressure fluctuations. *J. Fluid Mech.* **76**, 35–64.

WILLMARTH, W. W. & YANG, C. S. 1970 Wall-pressure fluctuations beneath turbulent layers on a flat plate and a cylinder. *J. Fluid Mech.* **41**, 47–80.

ZILBERMAN, M., WYGNANSKI, I. & KAPLAN, R. E. 1977 Transitional boundary layer spot in a fully turbulent environment. *Phys. Fluids* **20**, S258–271.